Magnetic nanoparticles through organometallic synthesis: evolution of the magnetic properties from isolated nanoparticles to organised nanostructures

Fréderic Dumestre,[ab] Susana Martinez,†[b] David Zitoun,[b] Marie-Claire Fromen,[c] Marie-José Casanove,[c] Pierre Lecante,[c] Marc Respaud,[d] Arnaud Serres,[d] Robert E. Benfield,[e] Catherine Amiens*[b] and Bruno Chaudret[b]

[a] *Digital DNA Labs, Semiconductor Products Sector, Motorola, le Mirail B.P. 1029, 31023 Toulouse, France*

[b] *Laboratoire de Chimie de Coordination, UMR 8241-CNRS, 205, Route de Narbonne, 31077 Toulouse Cedex 04, France. E-mail: amiens@lcc-toulouse.fr*

[c] *Centre d'Elaboration des Matériaux et d'Etudes Structurales, CNRS, 29, Rue Jeanne Marvig, BP 4347, 31055 Toulouse Cedex, France*

[d] *Laboratoire National des Champs Magnétiques Pulsés et Laboratoire de Physique de la Matière Condensée, INSA, 135 Av. de Rangueil, 31077 Toulouse, France*

[e] *Functional Materials Group, School of Physical Sciences, University of Kent, Canterbury, UK CT2 7NR*

Received 25th March 2003, Accepted 23rd April 2003
First published as an Advance Article on the web 28th August 2003

Co and NiFe nanoparticles (2.7 to 3.3 nm mean diameter) of narrow size distribution have been obtained through the decomposition of organometallic precursors in organic solutions of long alkyl chain ligands, namely oleic acid and hexadecylamine. Materials of various volume fractions were produced. The particles have been structurally characterised by WAXS. Both adopt the bulk structure: HCP in the case of cobalt; a mixture of FCC and BCC for NiFe. Their aptitude to self-assemble either on flat supports or in bulk solid state has been investigated by means of TEM and SAXS. This study suggests the crystallisation of the nanoparticles upon solvent evaporation, especially a local FCC arrangement was observed for the NiFe material. Magnetic measurements (SQUID) confirm this tendency. The blocking temperature depends on the metal volume fraction, *i.e.* on the anisotropy generated by the dipolar couplings (K_i). We show that, for dense samples, the particles of high intrinsic anisotropy, K_u, (Co) still display an individual behaviour while the soft ones (NiFe) display a collective behaviour.

† Present address: Laboratorio de Sintesis Organometalica, Escuela de Quimica, Facultad de Ciencias, UCV, 1041-A Caracas, Venezuela.

I. Introduction

Driven by potential applications in optics,[1] electronics[2] or magnetic data storage,[3] an important research effort has been directed towards the study of size controlled nanoparticles. Size reduction effects have been intensively studied on assemblies of isolated nanoparticles. However, packing of nanoparticles, which is mandatory in many applications, may greatly modify their individual behaviour.[4] For example, dipolar couplings or even exchange couplings may arise between magnetic particles.[5] If strong exchange or dipolar couplings take place, the magnetisation reversal process changes from rotation controlled to domain-nucleation controlled and thus a particle cannot be used as a unit cell for data storage. New magnetic behaviours are also expected for 2D assemblies: depending on the kind of arrangement the nanoparticles adopt on the surface, the dipolar interactions may be either demagnetising or magnetising, leading in the latter case to a ferromagnetic behaviour of the nanoparticle assembly.[6] Hence the control of the organisation of nanoparticles whether it is a self-assembly,[7] or induced by a specifically designed functionalisation of the particles[8] is very challenging.

One strategy to obtain regularly organised nanostructures is the synthesis of nanoparticles surrounded by ligands that promote their self-assembly, in general after size selection (to reduce the size dispersion to less than 5%), and help to control the distance between the nanoparticles.[9] Sun and Murray[10] have, for example, reported a high temperature preparation of 9 nm cobalt nanoparticles displaying a long-range self-organization. This method has been extended to the synthesis of Fe/Pt particles in order to increase the magnetic anisotropy of the materials with the goal of producing high-density memories.[11] Cobalt nanoparticles that self-assemble into 2D superlattices have also been reported by the group of Pileni by reverse micelle synthesis.[12] Recently, formation of 3D crystals of Co_3Pt and FePt nanoparticles has been achieved by very slow diffusion techniques by Rogach *et al.*[13]

The coordination of the ligands to the nanoparticles surface must not alter the intrinsic specific physical properties of the particles nor those induced by their nanometric size. This latter point is important in order to take advantage of both the intrinsic and collective properties for future applications.

Our group has developed an organometallic route towards the synthesis of metallic nanoparticles (such as Pt, Ru, Rh, Cu, In, Zn, PtRu, PdCu ...) of narrow size distribution.[14] This method has also been applied to the synthesis of magnetic nanoparticles of Co,[15] Ni,[16] or even bimetallic ones such as CoPt,[17] CoRh.[18] This method is based on the decomposition of an olefinic complex under a controlled atmosphere of H_2 in mild conditions of pressure. It was shown that the surface of the nanoparticles is free of contaminating agents: the magnetic properties are identical to those observed for nanoparticles produced and studied in ultra high vacuum.[19] Furthermore, we have demonstrated that σ-donor ligands such as amines or carboxylic acids do not alter the magnetic properties of the nanoparticles.[20] They are thus good candidates for the synthesis of ligand stabilised magnetic nanoparticles.

We report here the synthesis of magnetic Co and NiFe nanoparticles with sizes from 2.7 to 3.3 nm, stabilised by oleic acid or hexadecylamine and their structural characterisation by TEM and WAXS. We also discuss their self-assembly into 2D or 3D super-structures and long-range ordering on the basis of TEM and SAXS. We finally focus on the magnetic properties of the nanoparticle assemblies, especially those arising from magnetic couplings, and their effect on the effective anisotropy of the system, with respect to the average particle–particle distance, and to the organisation of the particles in the materials.

II. Synthesis and structural characterisation

Synthesis of magnetic nanoparticles is a difficult process. Thus, in addition to the control of the size and size distribution, magnetic couplings that tend to favour the agglomeration of the particles have to be dealt with. Moreover, the magnetic properties of such small particles highly depend on their surface state and the metals involved are extremely reactive towards dioxygen. A careful choice of the stabilising ligands and of the synthesis conditions is thus required. As already stated above, amines and carboxylic acids do not modify the surface magnetism of the particles.

Furthermore they have already been used to promote self-assembly of various nanoparticle systems[21] and exist with sufficiently long chains to avoid exchange coupling between the magnetic particles. Among the possible metal precursors, organometallic complexes with olefin or polyolefin ligands are the more interesting since they decompose easily and generate bare metal atoms and only alkanes as by-products. Olefinic precursors of cobalt: $Co(C_8H_{12})(C_8H_{13})$, synthesized according to published procedures[22] and nickel: $Ni(C_8H_{12})_2$, have been used here to synthesize magnetic nanoparticles of Co and, in association with $Fe(CO)_5$, NiFe nanoparticles. These precursors have already proven to be well adapted for the synthesis of size controlled nanoparticles.[15,16,20,23]

Two distinct procedures have been used. The cobalt precursor is very reactive and usually decomposes at room temperature. However, Co nanoparticles were obtained through hydrogenation (3 bar H_2) of the precursor in anisole, in the presence of oleic acid at 150 °C.[24] Very fast decomposition is observed. This, associated with a high nucleation rate ensures the formation of small particles. The decomposition leads only to cyclooctane as by product. The final material was recovered either by evaporation of the solvent and alkane to dryness **Co1,** or after precipitation of the concentrated crude solution into excess pentane **Co2**. The objective of the precipitation step was not to select the size of the particles but to get rid of excess ligand. Accordingly, compound **Co1** has very low cobalt content (10.4%) when comparing to **Co2** (48.8%). Moreover, some shadowy regions, corresponding to excess ligand, can be observed on the TEM[25] images of **Co1** (see Fig. 1).

On the contrary, the decomposition of the iron precursor requires thermal activation, even in the presence of the nickel organometallic complex. Furthermore, upon decomposition of the iron precursor, a large quantity of carbon monoxide is formed which could adsorb and react at the nanoparticles surface if not driven out of the reaction medium. Thus, to synthesise the NiFe nanoparticles, we refluxed a 1/1 mixture of the two precursors in anisole.[26] Hexadecylamine was chosen in this case to stabilise the particles, since it had already proven of good value in the stabilisation of nickel nanoparticles[20a] and was successfully used to induce long range self-assembly of In or Sn particles.[21] The solution turns black very quickly under these conditions. The reaction was monitored by IR spectroscopy, especially we have checked that there was no $Fe(CO)_5$ left in the medium after 3 h. The final material was recovered by evaporation of the solvent to dryness. No adsorbed CO could be evidenced at the nanoparticles surface by IR spectrocopy conducted on KBr pellets of the solid final material. Two different syntheses, following the same procedure, lead to two materials: **NiFe1** and **NiFe2** that differ only by the mean diameter of the particles. This point will be discussed later.

The chemical conditions used in these syntheses generate nanoparticles of narrow size distribution, as can be deduced from TEM images of the materials **Co1-2**, **NiFe1-2** and typical size histograms (Figs. 1–4). This is a great advantage for self-assembly, because it suppresses the time consuming and low yield size selection steps. Cobalt particles are obtained with two different sizes 2.5 and 3 nm for **Co1** and **Co2** respectively. **NiFe1** and **NiFe2** consist of NiFe nanoparticles of respectively 2.7 nm and 3.3 nm. The difference in size observed between **Co1** and **Co2,** should be

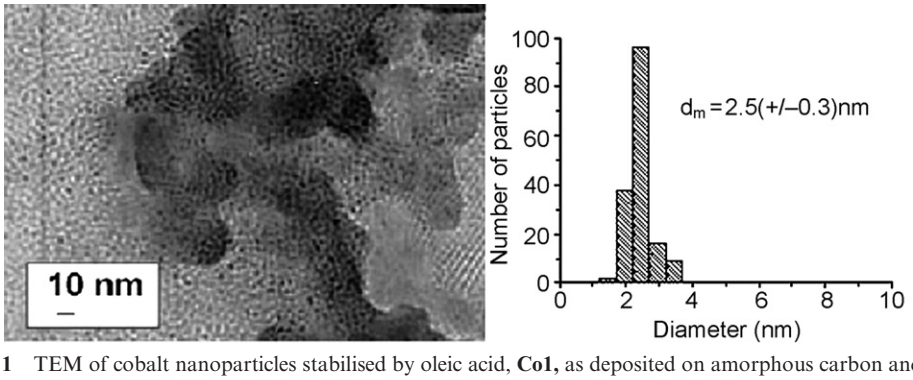

Fig. 1 TEM of cobalt nanoparticles stabilised by oleic acid, **Co1,** as deposited on amorphous carbon and size histogram.

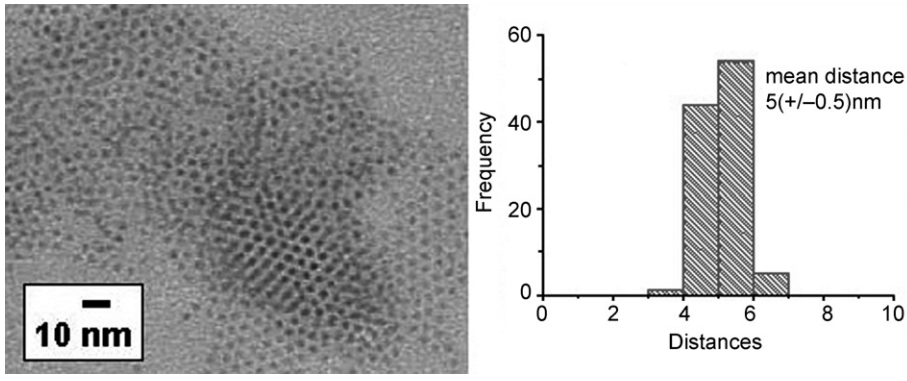

Fig. 2 TEM of cobalt nanoparticles stabilised by oleic acid, **Co2,** as deposited on amorphous carbon and distance histograms.

related to a slight difference in the heating process more than to the precipitation step, since no metal residue could be observed in the filtrate. The fact that the mean size of NiFe nanoparticles varies from one synthesis to the other can most probably be attributed to the same reason, as the nucleation process is the determining step and, unfortunately, yet the less controlled one.[7f,27]

Atomic structures within the nanoparticles have been further investigated by WAXS.[28] Cobalt nanoparticles display an HCP structure with parameters identical to that of bulk cobalt.[15b,20b] As can be deduced from Fig. 5 (bottom scheme), the radial distribution function (RDF) associated to NiFe nanoparticles displays a narrow first peak corresponding to a metal–metal bond of circa 251 pm, evidencing the metallic character of the particles. This RDF globally corresponds to that computed from a spherical particle with a FCC lattice; however the agreement is not perfect. Accordingly, the corresponding diffraction pattern, Fig. 5 (top scheme), displays peaks that correlate either to FCC or to BCC phases. For bulk NiFe, it has been reported that BCC and FCC phases coexist at low temperatures (below 250 °C) for Ni contents between 10 and 70%.[29] A similar behaviour is observed here for the NiFe nanoparticles. Distribution of both Ni and Fe in the particles is difficult to determine. However magnetic measurements,[30] especially the very low anisotropy value of these nanoparticles, are in good agreement with the formation of an alloy.

III. Organisation

The organisation of the particles has been investigated both on the crude powder by SAXS measurements and *via* TEM imaging of carbon coated copper grids on which a drop of a toluene solution of the material has been evaporated. No precaution was taken to control the evaporation rate of the solvent film.

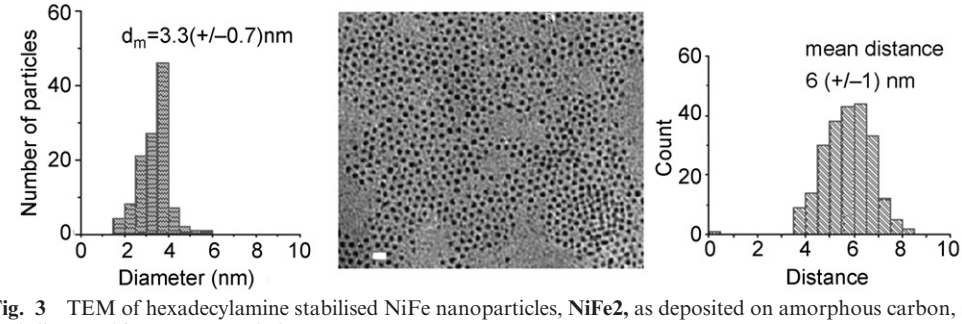

Fig. 3 TEM of hexadecylamine stabilised NiFe nanoparticles, **NiFe2,** as deposited on amorphous carbon, size and distance histograms. Scale bar: 10 nm.

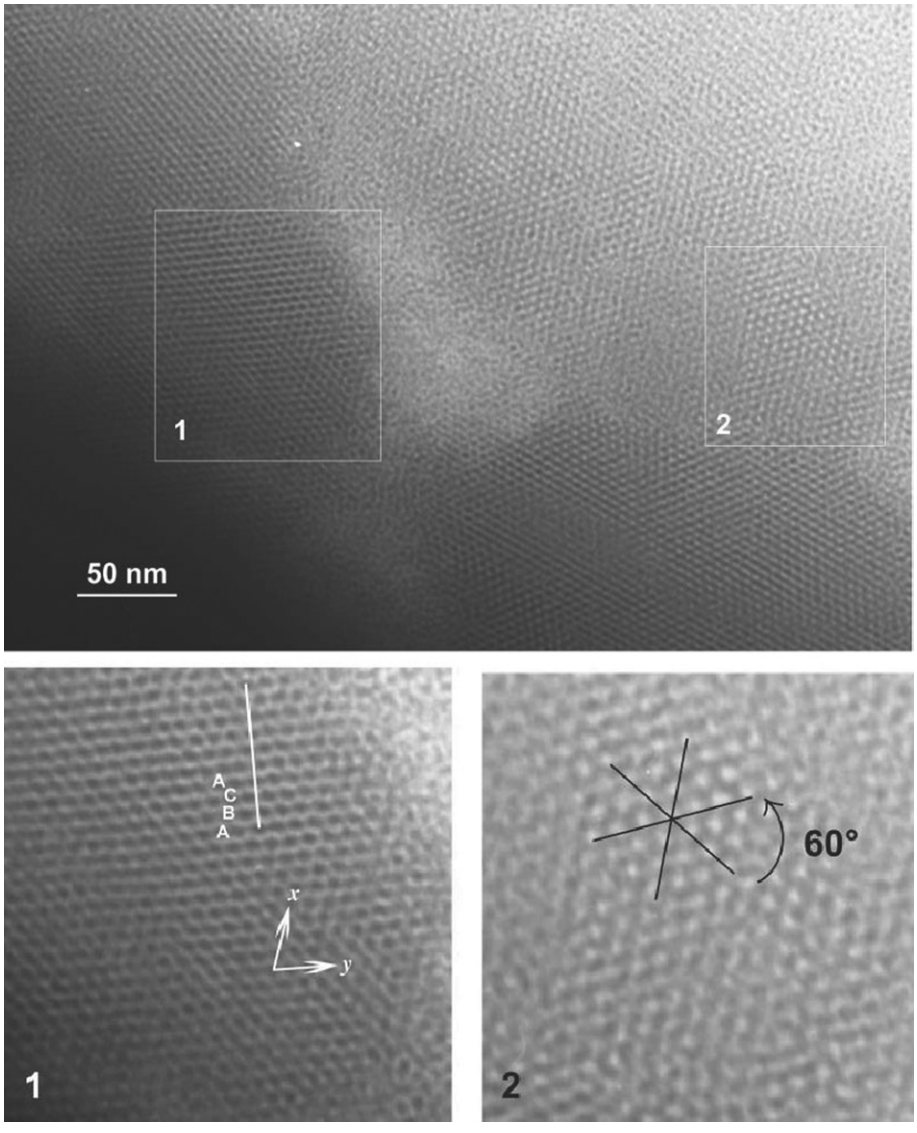

Fig. 4 TEM of hexadecylamine stabilised NiFe nanoparticles, **NiFe1,** as deposited on amorphous carbon. **1**: enlargement of region 1, showing the typical pattern of a FCC lattice observed along a [110] direction with the characteristic ABC stacking sequence of the (111) planes. However, the interparticle distance along the *x* and *y* directions ([112] directions in the FCC lattice) are slightly different: 4.9 nm in direction *x*, 5.2 nm along direction *y*. **2**: enlargement of region 2, showing a perfect hexagonal packing of the particles; the interparticle distance is 5.8 nm in all three directions, at 60° angles.

The different self-organisation patterns observed on the grids (Figs. 1–4) can be related to both the particle content in the material and the nature of the surrounding ligand. In the case of **NiFe2**, the organisation is scarce, most probably because of a slightly too broad size distribution. The mean distances between NiFe nanoparticles measured in dense regions fall on an average value of 6 nm (Fig. 3). From the mean diameter of these particles, 3.3 nm, we deduce an average spacing of 2.7 nm. As coordinated hexadecylamine extends its saturated alkyl chain to a maximum of 2.2 nm, the average spacing measured implies either constrained configurations for the alkyl chain or the occurrence of some interdigitation between the chains of adjacent particles.

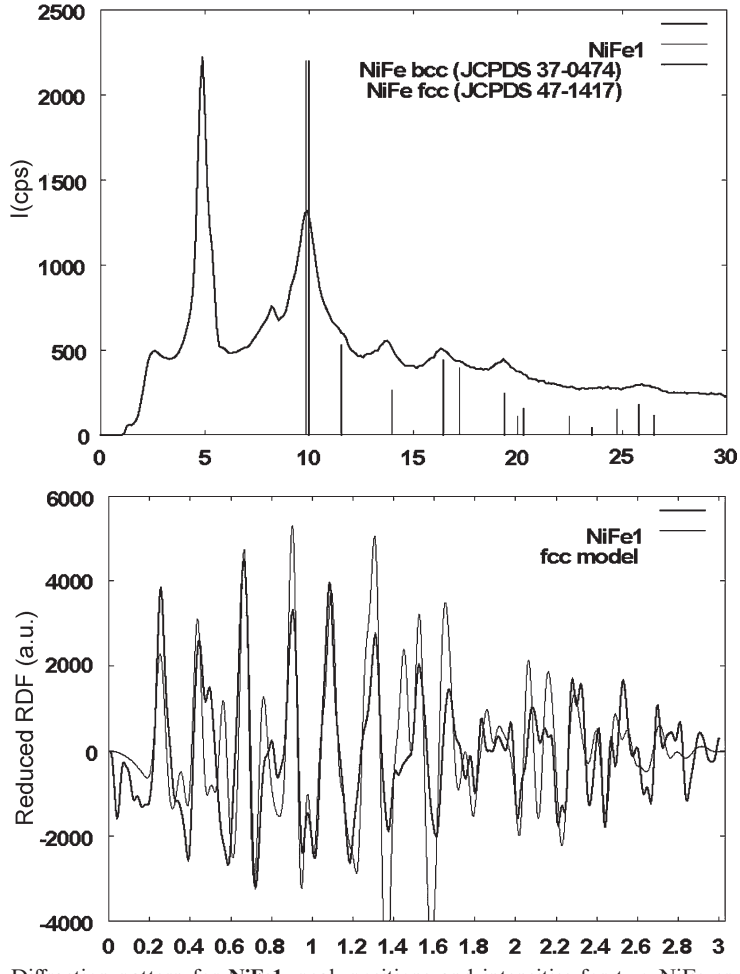

Fig. 5 Top: Diffraction pattern for **NiFe1**, peak positions and intensities for two NiFe crystalline samples (JCPDS files converted to molybdenum wavelength); bottom: Radial distribution function for **NiFe1** (full line) and computed from a spherical model (3 nm diameter) of FCC lattice (dotted line).

TEM investigation of NiFe nanoparticles from **NiFe1** shows that part of the grid is covered with monolayers of particles, adopting a perfect hexagonal packing, evidenced by the ABAB sequence and angles of 60 °C, as can be seen on the enlargement 2, Fig. 4. The interparticle distance is 5.8 nm in all three directions. Other regions consist of 3D assemblies, enlargement 1, Fig. 4. In this case, the particles layers are stacked along an ABCABC sequence, typical of a (111) plane stacking in a FCC lattice. The lattice is here observed along a [110] axis, and the x and y directions, which form an angle of 70°, correspond to [112] FCC directions. The interparticle distance however is different along the two directions (respectively 4.9 and 5.2 nm), which shows that the structure is slightly distorted. It is noteworthy that the directly observed lattice doesn't correspond to the compact lattice observed for monolayers and moreover that the interparticle distances are smaller than those measured on monolayers. This, along with the shape of the 3D regions, suggests that we are in the presence of crystallites formed during the evaporation process and subsequently deposited on the TEM grid. As these particles have a mean diameter of 2.7 nm, the average spacing in 3D crystallites is respectively of 2.2 and 2.3 nm, whereas in monolayers the average particle spacing has a value of 3.1 nm. This is in agreement with a strong interdigitation of the alkyl chains of the ligand in the case of the 3D crystallites, and further attests the idea of crystallisation in solution.[31] It is

noteworthy that spontaneous crystallisation of tin nanoparticles in the presence of hexadecylamine has already been observed in our group.[21]

In solution in a good solvent, and due to the high curvature of the nanoparticle surface, the alkyl chain of the ligand is very mobile.[32] This insures the stability of the colloidal solutions. Indeed, if the particles got close, the motions of the alkyl chain would be restricted, which is not favourable from an entropic point of view, moreover osmotic effects would also tend to repel the particles. However, as the solvent evaporates the particles are forced to get close to one another. Van der Waals interactions, either between the particles metallic core or between the alkane chains, can take place. The interdigitation process would then favour these Van der Waals interactions inducing crystallisation of the alkyl chain in the particle interspacing and crystallization of the particle assembly.

In the case of cobalt nanoparticles protected by oleic acid, the TEM images display different patterns according to the metal content in the sample. As already mentioned above, almost no organisation is observed when a large excess ligand is present in the material (Fig. 1). However, for **Co2**, the particles tend to form hexagonal arrays on the grid (Fig. 2). Oleic acid has a long olefinic chain (C18) which presents a double bond at the C9 position with a *cis* configuration. The induced kinking of the carbon tail has been suggested to be at the origin of the good stabilising properties of this ligand.[23] The apparent length of the alkyl chain thus more or less corresponds to that of a C9 carboxylic acid, *i.e.* 1.4 nm at maximum extension when coordinated at a metal surface. However, the packing of the bent part of the chains over the particle surface clearly prevents any interdigitation between the ligand chains of different particles. The mean interparticle distance between the particles deposited on the amorphous carbon grid corresponds to approximately 5 nm, leading to spacing of 2 nm, clearly indicating a collapse of the alkyl chains of the ligand. This collapse most probably occurs upon evaporation of the solvent. It has already been observed during the formation of assemblies of functionalized gold nanoparticles.[8d]

Local arrangement is close to hexagonal in both cases, with multiple stacking faults.

For comparison one drop of the same solution was deposited on freshly cleaved carbon graphite. In Fig. 6, we can see that the organisation pattern is similar to what is observed on amorphous carbon. However, formation of multilayers is more often observed in this case.

The formation of superlattices is the result of competing forces: repulsive forces discussed above, Van der Waals attractive forces between the particles, magnetic interactions, and surface tension during evaporation. At a given temperature, *i.e.* thermal energy motion, the time allowed to the evaporation process is crucial: the particles should have enough time to find their equilibrium position, like in a crystallisation process, if a close-packed lattice is expected to form. This can be particularly difficult for small particles, where Van der Waals interactions between the metallic cores are very small.[33] Furthermore, in these experiments, no precaution was taken to control the evaporation rate of the solvent. This could be a possible reason for the numerous stacking faults observed in the particle assembly.

SAXS measurements have been performed on the solid samples.[34] In *k*-space, a sharp peak is observed for each sample at a value between 1.8 and 1.25 nm^{-1}, as well as a broad one at 0.86 nm^{-1} in the case of **NiFe1-2**. The corresponding distances are respectively 5.3 to 5 and 7.3 nm.

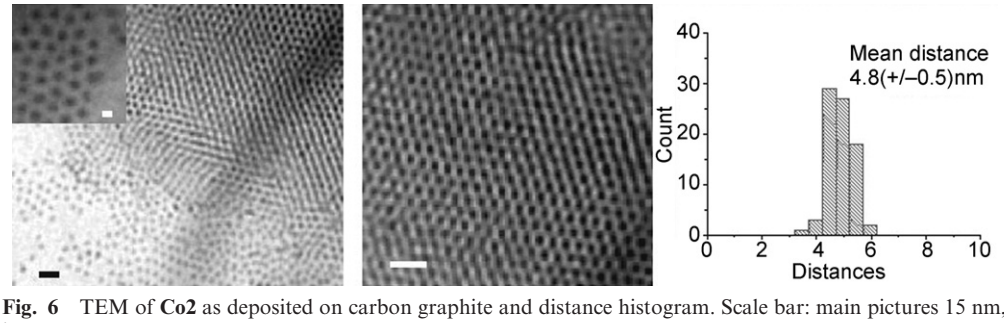

Fig. 6 TEM of **Co2** as deposited on carbon graphite and distance histogram. Scale bar: main pictures 15 nm, insert: 3 nm.

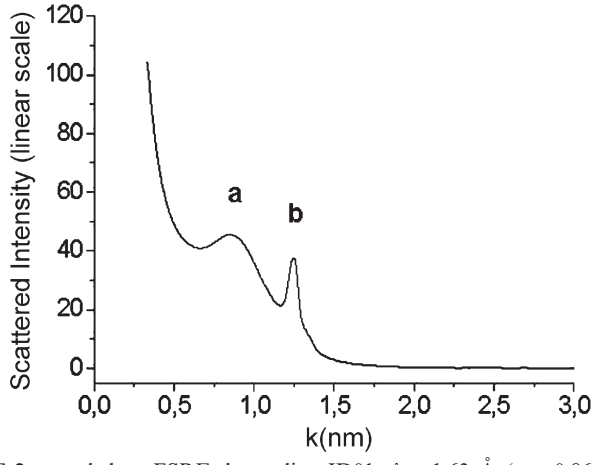

Fig. 7 SAXS of **NiFe2** recorded at ESRF, beam line ID01, $\lambda = 1.63$ Å ($a = 0.86$ nm^{-1}; $b = 1.25$ nm^{-1} corresponding respectively to distances of 7.3 nm and 5 nm).

Fig. 7 displays the data set for **NiFe2**, after correction from the background scattering. We tentatively attribute these distances to interparticle distances. They are in good agreement with the interparticle distances measured by TEM on Co nanoparticles protected by oleic acid and with those measured in 3D crystallites of **NiFe1**. It is noteworthy that in the case of **NiFe2**, the first average particle–particle distance is smaller in the solid state than what can be measured on the TEM grid. We relate this to a possible interdigitation, or at least a different conformation, of the alkyl chains in the solid state. This can be also related to a collapse of the alkyl chain during the drying step. It further suggests that the solid may contain small crystallites as observed for **NiFe1**.

The broad peak could correspond to less dense regions in the powder or to distances between second neighbours. The absence of peaks at lower k-values, for each sample, evidences the absence of long range order in the solids.

IV. Magnetic properties

The nanoparticles described herein are small enough to be regarded as single domain magnetic particles. Magnetic studies were carried out on dried samples.[35] In Fig. 8 we show the zero field cooling/field cooling (ZFC-FC) curves for the three colloids. As a common feature their shapes evidence a single maximum on the ZFC curve at a temperature T_B and increasing susceptibility when lowering the temperature on the FC curves. Such behaviour is characteristic of superparamagnetism. In each case when lowering the temperature, the FC curve follows the ZFC one and deviates at a temperature very close to T_B.

Superparamagnetism was also confirmed by the isothermal magnetisation measurements. For each compound the magnetisation curve measured at a temperature below the blocking temperature T_B is hysteristic (not shown). The hysteristic behaviour disappears for temperatures above T_B. From the values of the magnetisation measured at 5 K and 5 T and the metal ratio determined by chemical analysis, we estimated the values of the average magnetic moment per cobalt atom to be 1.72($\pm$0.1) μ_B/Co atom for **Co1** and **Co2** and 1.15($\pm$0.1) μ_B/average metal atom for **NiFe2**. The measured value for the Co corresponds to the bulk one as expected for cobalt particles stabilised by a carboxylic acid. The magnetic moment per average metal atom measured for the NiFe nanoparticles is significantly below the expected bulk value (1.7 μ_B/atom). The origin of this reduction is not yet clearly established. The chemical elaboration of iron based nanoparticles without any surface contamination remains a challenge. In the present case, the decomposition of the $Fe(CO)_5$ precursor generates carbon monoxide that could be partially trapped at the particle surface, despite the careful conditions used for the synthesis. Carbon monoxide could also react with the particles

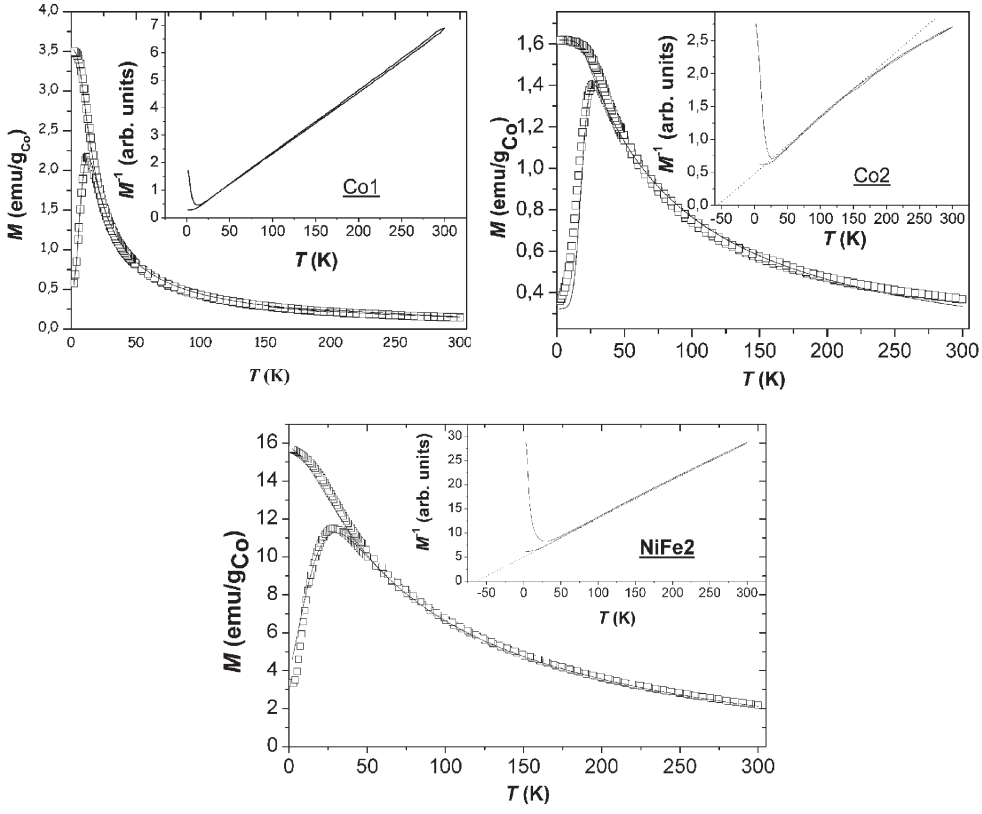

Fig. 8 ZFC/FC curves for **Co1-2** and **NiFe2** materials recorded on powders. (Symbols: experimental data; straight lines: best fit, see text.)

to form surface carbides and/or oxides. As no CO could be evidenced at the surface of the particle by IR spectroscopy, the second hypothesis is likely to be responsible for the observed decrease of the local magnetic moment. These aspects will be discussed elsewhere. In this paper, we will focus on the role of long range dipolar magnetic interactions on the blocking temperature. In particular, we will examine what is the influence of the intrinsic anisotropy of the particles, and that of the magnetic interactions on the magnetisation process.

The influence of the increase of the nanoparticles concentration could be first identified on the susceptibility. For systems of non-interacting magnetic nanoparticles, the susceptibility follows a simple Curie law above the blocking temperature. In this temperature range, when magnetic interactions are present, the variation of the magnetisation (m) as a function of the temperature (T) measured in a low magnetic field (H) follows a Curie–Weiss law,

$$m = \text{constant} \times \frac{H}{T - \theta},$$

where θ reflects the strength of the magnetic interactions. For **Co1** and **NiFe2**, the inverse of m *versus* T follows a straight line which allows one to determine precisely the values of θ, respectively -4 K and -60 K (see insert, Fig. 8). For **Co2**, the Curie–Weiss behaviour is less evident and only an average value of -55 K can be estimated (insert, Fig. 8). We can observe that according to the increase of the magnetic volume fraction, the strength of the dipolar interactions increases.

In order to analyse these data more precisely, we have fitted the experimental curves for the three samples using the model described hereafter.

We assume that ZFC magnetisation and FC magnetisation both result from superparamagnetic and blocked contributions, as described in the following expressions:

$$m_{\mathrm{ZFC}} = \frac{M_{\mathrm{S}}^2(T)H}{3V}\left[\frac{1}{k_{\mathrm{B}}(T-\theta)}\int_0^{v_{\mathrm{m}}(T)} v^2 \mathrm{f}(v)\mathrm{d}v + \frac{1}{3K_{\mathrm{eff}}}\int_{v_{\mathrm{m}}(T)}^{\infty} v\mathrm{f}(v)\mathrm{d}v\right],$$

$$m_{\mathrm{FC}} = \frac{M_{\mathrm{S}}^2(T)H}{3V}\left[\frac{1}{k_{\mathrm{B}}(T-\theta)}\int_0^{v_{\mathrm{m}}(T)} v^2 \mathrm{f}(v)\mathrm{d}v + \frac{\ln(\tau_{\mathrm{m}}/\tau_0)}{3K_{\mathrm{eff}}}\int_{v_{\mathrm{m}}(T)}^{\infty} v\mathrm{f}(v)\mathrm{d}v\right],$$

where $V = \int_0^{\infty} v\mathrm{f}(v)\mathrm{d}v$, M_{S} is the spontaneous magnetisation, $v_{\mathrm{m}}(T)$ is the transition volume above which the particle is in the blocked state, below which the particle is in the superparamagnetic state.

In the case of a system of interacting magnetic particles, the relaxation time (τ) associated to the superparamagnetic behaviour is defined by,

$$\tau = \tau_0 \exp\left(\frac{K_{\mathrm{eff}} v}{k_{\mathrm{B}}(T-\theta)}\right),$$

where $\tau_0 = 10^{-9}$ s. For a measurement time of $\tau_{\mathrm{m}} = \tau$, $v_{\mathrm{m}}(T)$ is defined as

$$v_{\mathrm{m}}(T) = \ln\left(\frac{\tau_{\mathrm{m}}}{\tau_0}\right)\frac{k_{\mathrm{B}}(T-\theta)}{K_{\mathrm{eff}}}.$$

Using the Weiss temperature deduced from the $m^{-1}(T)$ curves, we then fit the ZFC/FC curves using a Log-normal size distribution (f(v)) of particles to describe the magnetic size distributions.

A very good fit was achieved for all three systems, allowing accurate determination of the effective anisotropy (K_{eff}). The parameters used are listed in Table 1.

We can observe that the magnetic size, *i.e.* the average size activated in the superparamagnetic relaxation, is identical to that measured by TEM for the **Co1-2** samples, within experimental errors. The effective anisotropy is much higher for the system of higher magnetic volume fraction. This increase can be ascribed to the influence of the magnetic dipolar interactions, which give a contribution to the total anisotropy barrier (K_{i}). The second contribution is due to the intrinsic anisotropy of the nanoparticles (K_{u}). Taking into account the value of the intrinsic effective magnetic anisotropy (K_{u}) measured in non-interacting system, which is close to the bulk one (4×10^6 erg cm^{-3}), we calculated the value of K_{i} from the expression $K_{\mathrm{eff}} = K_{\mathrm{u}} + K_{\mathrm{i}}$. The calculated values for K_{i} are thus 10^6 erg cm^{-3} and 7×10^6 erg cm^{-3} for **Co1** and **Co2** respectively. K_{i} can be related to the magnetic volume fraction through the expression derived by Dorman *et al.*, $K_{\mathrm{i}} = naM_{\mathrm{S}}^2$,[36] where n is the number of first nearest neighbours, and a, the magnetic volume fraction. Considering a compact packing with $n = 12$, the magnetic volume fractions a are estimated to 5% and 30% for **Co1** and **Co2** respectively. Actually, sample **Co2** has the higher metal content, with a volume fraction close to 10%. On the contrary, sample **Co1** consists of diluted nanoparticles with a volume fraction of 1%. Both the SAXS and magnetic measurements evidence more dense regions, pointing to a non-homogeneous sample. We tentatively relate this to a beginning of organisation and to the presence of excess ligand.

The NiFe sample, **NiFe2**, displays a much more complicated behaviour. The activated volume involved in the superparamagnetic regime is much larger than the volume calculated from TEM observations. In this system, the intrinsic anisotropy of the particles is small (close to 10^4 erg cm^{-3} in the bulk),[3a] and thus the main contribution to the effective anisotropy is due to the magnetic dipolar anisotropy, which value can be estimated close to 2.9×10^6 erg cm^{-3}. The value obtained for the magnetic volume fraction falls around 28% which is consistent with the structural data (22%). However this is much higher than the 1% value deduced from the micro-analysis on the basis of a homogeneous material. The higher magnetic volume fraction is a further evidence that these nanoparticles tend to crystallise.

It is difficult to interpret the role of dipolar interactions on the blocking temperature on the basis of this sole set of experiments. However, its first influence leads to an increase of the blocking temperature, as can be seen for **Co1-2** samples. Furthermore, it is interesting to compare the two samples with the higher magnetic volume fraction: **Co2** and **NiFe2**. The large magnetic volume determined in the case of **NiFe2** can be interpreted as an evidence of the simultaneous rotation of

Table 1 Main characteristics of **Co1-2** and **NiFe1-2** materials

		Interparticle distance/nm			f(v)					
Material	Diameter/nm	SAXS	TEM	T_B/K	ϕ_0/nm	σ	K_{eff}/erg cm^{-3}	K_u/erg cm^{-3}	K_i/erg cm^{-3}	θ/K
Co1	2.5	5.3	–	12	2.4	0.1	5.0×10^6	4.0×10^6	1.0×10^6	−4
Co2	3.0	5.3	−5	28	3.4	0.02	11×10^6	4.0×10^6	7.0×10^6	−55
NiFe1	2.7	5. 2	−5.8 or 4.9 and 5.2	—	—	—	—	—	—	—
NiFe2	3.3	5 and 7.3	−6	28	5.5	0.06	3×10^6	$< 10^5$	$\approx 2.9 \times 10^6$	−60

several particles. The rotation of the magnetisation seems to remain individual in the case of **Co2**. The main difference between these two samples consists in the hard and soft characters of Co and NiFe respectively. Thus, it seems that the hard intrinsic anisotropy preserves the individual behaviour, while soft systems display an easier transition to the collective one. These tendencies must be checked on a wider range of systems of various intrinsic anisotropies and various volume fractions, in order to have a more precise picture.

From the theoretical point of view, these phenomenons are not well identified. The magnetisation process of such materials cannot be described by analytical models. Monte-Carlo calculations have demonstrated their ability to simulate the magnetic properties of non-interacting nanoparticles.[37] The case of interacting nanoparticles is more difficult to address since it requires the calculation at each nanoparticle site of the local field due to the long range dipolar fields. Preliminary calculations have been performed in order to investigate the role of the interparticle distance on a system of Co nanoparticles with a HCP crystallisation, in agreement with published works.[38] Qualitatively, the first clear tendency is that, increasing the magnetic volume fraction leads to an increase of the blocking temperature as can be observed experimentally on **Co1-2** samples. Further calculations are in progress in order to determine precisely the influence of K_i/K_u on the magnetization process, especially, the activated volume and correlation length.

V. Conclusion

We have synthesised nanoparticles of Co and NiFe displaying narrow size distributions. The stability and size control was achieved by use of oleic acid in the case of the Co particles and hexadecylamine in the case of NiFe particles. Structural and magnetic measurements show that these particles tend to self-assemble either when deposited on carbon surfaces or in the solid state during the evaporation process. Especially, in the case of NiFe capped by hexadecylamine, nanocrystallites probably form spontaneously from the solution, which implies a precise positioning of the particles. This could be related to the magnetic properties of the particles assemblies. Interestingly, we have found that the magnetic behaviour of the particles varies from an individual to a collective one, as the anisotropy ratio K_i/K_u increases. This is particularly important if applications in data storage are aimed at. Materials with high anisotropy will both allow decreasing the critical size of the magnetic dot and help maintain an individual behaviour even if strong dipolar couplings are present, as it will be the case for high density media. These tendencies must be confirmed by analysing the influence of the anisotropy ratio K_i/K_u on the magnetization process, on different materials with different magnetic volume fraction.

Acknowledgements

The authors thank Alain Mari for recording the magnetic measurements, Vincent Colliere for technical assistance in TEM imaging. We gratefully acknowledge financial support from CNRS and Motorola and the Cooperation Program PCP "Nanosystèmes-Nanomesures" between Venezuela (Fonacit) and France (Ministère des Affaires étrangères).

References

1 (*a*) Z.-Z. Gu, R. Horie, S. Kubo, Y. Yamada, A. Fujishima and O. Sato, *Angew. Chem., Int. Ed. Engl.*, 2002, **41**, 1153; (*b*) Y. Lu, Y. Yin, Z.-Y. Li and Y. Xia, *Nano Lett.*, 2002, **2**, 785; (*c*) G. Santamaria, V. Salgueirino-Maceira, C. Lopez and L. M. Liz-Marzan, *Langmuir*, 2002, **18**, 4519.

2 (*a*) S. Liu, R. Maoz, G. Schmid and J. Sagiv, *Nano Lett.*, 2002, **2**(10), 1055; (*b*) U. Simon, *Adv. Mater.*, 1998, **10**, 1487; (*c*) D. L. Klein, R. Roth, A. K. L. Lim, A. P. Alivisatos and P. L. McEuen, *Nature*, 1997, **389**, 699.

3 (*a*) *Modern Magnetic Materials*, ed. R. C. O'Handley, Wiley-Interscience, New-York, 1999; (*b*) *Clusters and Colloids. From theory to applications*, ed. G. Schmid, VCH, Wienheim, 1994.

4 (*a*) M.-P. Pileni, *J. Phys. Chem. B*, 2001, **105**, 3358; (*b*) A. A. Mikhailovsky, A. V. Malko, J. A. Hollingsworth, M. G. Bawendi and V. I. Klimov, *Appl. Phys. Lett.*, 2002, **80**(13), 2380.

5 (*a*) H. Zeng, S. Sun, T. S. Vedantam, J. P. Liu, Z.-R. Dai and Z.-L. Wang, *Appl. Phys. Lett.*, 2002, **8**(14), 2583; (*b*) H. Zeng, J. Li, Z. L. Wang and S. Sun, *Nature*, 2002, **420**, 395.

6 (*a*) V. F. Puntes, K. M. Krishnan and P. Alivisatos, *Appl. Phys. Lett.*, 2001, **78**(15), 2187; (*b*) J. Legrand, C. Petit, D. Bazin and M.-P. Pileni, *Appl. Surf. Sci.*, 2000, **164**, 186; (*c*) V. Russier, C. Petit, J. Legrand and M.-P. Pileni, *Appl. Surf. Sci.*, 2000, **164**, 193.
7 (*a*) I. Sloufova-Srnova and B. Vlckova, *Nano Lett.*, 2002, **2**, 121; (*b*) S. Kang, J. W. Harrell and D. E. Nikles, *Nano Lett.*, 2002, **2**, 1033; (*c*) M. Chen and D. E. Nikles, *Nano Lett.*, 2002, **2**, 211; (*d*) D. V. Talapin, E. V. Shevchenko, A. Kornowski, N. Gaponik, M. Haase, A. L. Rogach and H. Weller, *Adv. Mater.*, 2001, **13**, 1868; (*e*) S. L. Tripp, S. V. Pusztay, A. E. Ribbe and A. Wei, *J. Am. Chem. Soc.*, 2002, **124**, 7914; (*f*) V. F. Puntes, D. Zanchel, C. K. Erdonmez and A. P. Alivisatos, *J. Am. Chem. Soc.*, 2002, **124**, 12 874; (*g*) M. T. Reetz, M. Winter and B. Tesche, *Chem. Commun.*, 1997, 147; (*h*) P. J. Thomas, G. U. Kulkarni and C. N. R. Rao, *J. Phys. Chem. B*, 2000, **104**, 8138.
8 (*a*) K. Akamatsu, J. Hasegawa, H. Nawafune, H. Katayama and F. Ozawa, *J. Mater. Chem.*, 2002, **12**, 2862; (*b*) L. Nagle, D. Ryan, S. Cobbe and D. Fitzmaurice, *Nano Lett.*, 2003, **3**, 51; (*c*) S. Gomez, L. Erades, K. Philippot, B. Chaudret, V. Colliere, O. Balmes and J.-O. Bovin, *Chem. Commun.*, 2001, **16**, 1474; S. Cobbe, S. Connolly, D. Ryan, L. Nagle, R. Eritja and D. Fitzmaurice, *J. Phys. Chem. B*, 2003, **107**, 470; (*d*) T. B. Norsten, B. L. Frankamp and V. M. Rotello, *Nano Lett.*, 2002, **2**, 1345; (*e*) S. Mann, S. A. Davis, S. R. Hall, M. Li, K. H. Rhodes, W. Shenton, S. Vaucher and B. Zhang, *J. Chem. Soc., Dalton Trans.*, 2000, 3753.
9 J. E. Martin, J. P. Wilcoxon, J. Odinek and P. Provencio, *J. Phys. Chem. B*, 2000, **104**, 9475.
10 S. Sun and C. B. Murray, *J. Appl. Phys.*, 1999, **85**, 4325.
11 S. Sun, C. B. Murray, D. Weller, L. Folks and A. Moser, *Science*, 2000, **287**, 1989.
12 J. Legrand, A. T. Ngo, C. Petit and M. P. Pileni, *Adv. Mater.*, 2001, **13**, 58.
13 (*a*) E. V. Shevchenko, D. V. Talapin, A. L. Rogach, A. Kornowski, M. Haase and H. Weller, *J. Am. Chem. Soc.*, 2002, **124**, 11 480; (*b*) E. V. Shevchenko, D. V. Talapin, A. Kornowski, F. Wiekhorst, J. Kötzler, M. Haase, A. L. Rogach and H. Weller, *Adv. Mater.*, 2002, **14**, 286.
14 (*a*) C. Amiens, D. de Caro, B. Chaudret and H. Wally, *J. Chem. Soc., Chem. Commun.*, 1994, 1891; A. Rodriguez, C. Amiens, B. Chaudret and J. S. Bradley, *Chem. Mater.*, 1996, **8**, 1978; (*b*) R. Choukroun, D. de Caro, S. Mateo, C. Amiens, B. Chaudret, E. Snoeck and M. Respaud, *New J. Chem.*, 2001, **25**, 525; (*c*) K. Soulantica, A. Maisonnat, M.-C. Fromen, M.-J. Casanove, P. Lecante and B. Chaudret, *Angew. Chem., Int. Ed. Engl.*, 2001, **40**, 448; (*d*) F. Rataboul, C. Nayral, M.-J. Casanove, A. Maisonnat and B. Chaudret, *J. Organomet. Chem.*, 2002, **643–644**, 307.
15 (*a*) J. Osuna, D. de Caro, C. Amiens, B. Chaudret, E. Snœck, M. Respaud, J.-M. Broto and A. Fert, *J. Phys. Chem.*, 1996, **100**, 14 571; (*b*) F. Dassenoy, M.-J. Casanove, P. Lecante, M. Verelst, E. Snoeck, A. Mosset, T. Ould Ely, C. Amiens and B. Chaudret, *J. Chem. Phys.*, 2000, **112**, 8137–8145.
16 T. Ould Ely, C. Amiens, B. Chaudret, E. Snoeck, M. Verelst, M. Respaud and J.-M. Broto, *Chem. Mater.*, 1999, **11**, 526.
17 T. Ould Ely, C. Pan, C. Amiens, B. Chaudret, F. Dassenoy, P. Lecante, M.-J. Casanove, A. Mosset, M. Respaud and J.-M. Broto, *J.Phys. Chem.*, 2000, **104**, 695.
18 D. Zitoun, M. Respaud, C. Amiens, B. Chaudret, A. Serres, M.-J. Casanove, M.-C. Fromen and P. Lecante, *Phys. Rev. Lett.*, 2002, **89**, 37 203.
19 M. Respaud, J.-M. Broto, H. Rakoto, A. Fert, M. Verelst, E. Snoeck, P. Lecante, A. Mosset, L. Thomas, B. Barbara, J. Osuna, T. Ould Ely, C. Amiens and B. Chaudret, *Phys. Rev. B*, 1998, **57**, 2925.
20 (*a*) N. Cordente, C. Amiens, M. Respaud, F. Senocq, M.-J. Casanove and B. Chaudret, *Nano Lett.*, 2001, **1**, 526; (*b*) F. Dumestre, B. Chaudret, C. Amiens, M.-C. Fromen, M.-J. Casanove, P. Renaud and P. Zurcher, *Angew. Chem., Int. Ed. Engl.*, 2002, **41**(22), 4286.
21 (*a*) K. Soulantica, A. Maisonnat, F. Senocq, M.-C. Fromen, M.-J. Casanove and B. Chaudret, *Angew. Chem., Int. Ed. Engl.*, 2001, **40**(16), 2984; (*b*) K. Soulantica, A. Maisonnat, M.-C. Fromen, M.-J. Casanove and B. Chaudret, *Angew. Chem.*, 2003, **42**, 1945.
22 S. Otsuka and M. Rossi, *J. Chem. Soc. A*, 1968, 2630.
23 K. S. Suslick, M. Fang and T. Hyeon, *J. Am. Chem. Soc.*, 1996, **18**(47), 11 960.
24 The reaction is conducted under argon to avoid any surface oxidation of the particles. In a typical experiment, 1 mmol $Co(C_8H_{12})(C_8H_{13})$ was decomposed in 20 mL anisole at 150 °C under 3 bar H_2, in the presence of one equivalent oleic acid. After 48 h, the solvent is either evaporated to dryness, leading to sample **1**; or the solution is concentrated and poured into a large volume of cold pentane to ensure precipitation of the particles (sample **2**). Cobalt content in each sample was determined by chemical microanalysis at the CNRS center, Vernaison, France.
25 Transmission electron microscopy (TEM) was used to determine both particle size, size distribution and interparticle distances. Low-resolution TEM measurements were performed on a JEOL 200 CX (200 kV) at the TEMSCAN facility, Université Paul-Sabatier, Toulouse. More than 200 particles were measured to draw each size or distance histogram.
26 In a typical experiment, a 1/1 mixture of the two precursors ($Ni(COD)_2$, $Fe(CO)_5$) in anisole was heated at reflux for 3 h in the presence of one equivalent (*versus* the total metal content) of HDA. During this time the initial orange solution turns black. The reaction is conducted under argon to avoid any surface oxidation of the particles. After evaporation of the crude solution to dryness, the solid material has been characterised without further purification step. The nickel and iron contents were determined by chemical microanalysis. Ni: 6.85% Fe: 5.67%. (*i.e.* metal content 12.52%).

27 Z. A. Peng and X. Peng, *J. Am. Chem. Soc.*, 2002, **124**, 3343.
28 WAXS structural characterisations by WAXS were performed in the solid state. The fine powder was introduced in a thin walled Lindemann capillary of 1 mm diameter subsequently sealed under argon. Measurements of the X-ray intensity scattered by the samples irradiated with graphite-monochromatised molybdenum Kα radiation (0.071069 nm) were performed using a dedicated two-axis diffractometer. Fluorescence from iron and nickel was removed at the measurement step by filtering. Time for data collection was typically 20 h for a set of 457 measurements collected at room temperature in the range $0° < \theta < 65°$ for equidistant s values [$s = 4\pi(\sin\theta/\lambda)$].
29 F. Lihl, *Arch. Eisenhüttenwes.*, 1954, **25**, 475.
30 To be published.
31 FCC packing of nanoparticles, resulting from layer by layer growth on a compact 2D assembly of particles, has already been reported. In this case the interparticle spacings were identical in 2D and 3D assemblies; (*a*) A. Korgel, S. Fullam, S. Connolly and D. Fitzmaurice, *J. Phys. Chem. B*, 1998, **102**, 8379; (*b*) M. P. Pileni, *J. Phys. Chem. B*, 2001, **105**, 3358.
32 (*a*) F. Dassenoy, K. Philippot, T. Ould Ely, C. Amiens, P. Lecante, E. Snoeck, A. Mosset, M.-J. Casanove and B. Chaudret, *New J. Chem.*, 1998, **22**, 703; (*b*) C. Pan, K. Pelzer, K. Philippot, B. Chaudret, F. Dassenoy, P. Lecante and M.-J. Casanove, *J. Am. Chem. Soc*, 2001, **123**, 7584.
33 G. Viau, R. Brayner, L. Poul, N. Chakroune, E. Lacaze, F. Fiévet-Vincent and F. Fiévet, *Chem. Mater.*, 2003, **15**, 486.
34 The SAXS experiments were conducted on beamline ID01 at the European Synchrotron Radiation Facility (ESRF), Grenoble, France (ESRF web site: http//www.esrf.fr/exp_facilities/ID1/user_guide/), operating under beam conditions of 6 GeV, 200 mA, and 2/3 filling mode. The X-ray energy was 7610 eV, corresponding to a wavelength of 1.629 Å. A beam size 0.8 mm × 0.2 mm was used. The samples were contained in thin walled Lindemann capillaries of 1 mm diameter sealed under argon mounted horizontally perpendicular to the X-ray beam. The samples were at ambient temperature. The SAXS intensity profiles were measured with a CCD detector, with an active array of 1242 × 1152 pixels each of 55 μm × 55 μm. The central area was masked by a beam stop 6 mm in diameter. The detector was positioned at distances between 0.6 m and 4.5 m from the sample, giving a range for the scattering vector k of up to 3.0 nm^{-1}. Typical counting times for the 0.6 m detector position were 2.5 min. Background counts, recorded with an empty sample tube, were very low and showed no specific features. The 2D-diffraction patterns were radially integrated using the software package FIT2D (A. P. Hammersley, *ESRF Internal Report, ESRF97HA02T*, 1997, "FIT2D: An Introduction and Overview") to display the intensity profile as a function of the scattering angle or vector.
35 Magnetisation measurements were performed on a SQUID magnetometer (MPMS Quantum Design). The temperature was varied between 2 and 300 K according to a classical zero field cooling/field cooling (ZFC/FC) procedure in the presence of a very weak applied magnetic field (10 Oe) and the hysteresis cycles were obtained at different temperatures in a magnetic field varying from + 50 to −50 kOe. The samples were prepared in gelatine capsules in a glove box to avoid any oxidation of the materials.
36 J. L. Dormann, F. D'Orazio, F. Lucarri, E. Tronc, P. Prené, D. Fiorani, D. Cherkaoui and R. Noguès, *Phys. Rev. B*, 1996, **53**, 14 291.
37 D. A. Dimitrov and G. M. Wysin, *Phys. Rev. B*, 1996, **54**, 9237.
38 (*a*) D. Kekrachos and N. K. Trohidou, *Phys. Rev. B*, 1998, **58**, 12 169; (*b*) R. W. Chantrell, N. Walmsley, J. Gore and M. Maylin, *Phys. Rev. B*, 2000, **63**, 24 410; (*c*) C. Binns, M. J. Maher, Q. A. Pankhurst, D. Kechrakos and K. N. Trohidou, *Phys. Rev. B*, 2002, **66**, 184 413.